Hindawi Publishing Corporation
Advances in Materials Science and Engineering
Volume 2010, Article ID 681574, 15 pages
doi:10.1155/2010/681574

Research Article

A Phenomenological Study on the Synergistic Role of Precious Metals and the Support in the Steam Reforming of Logistic Fuels on Monometal Supported Catalysts

Abdul-Majeed Azad and Desikan Sundararajan

Chemical Engineering Department, The University of Toledo, 2801 W. Bancroft St., Toledo, OH 43606-3390, USA

Correspondence should be addressed to Abdul-Majeed Azad, abdul-majeed.azad@utoledo.edu

Received 30 January 2010; Accepted 8 May 2010

Academic Editor: Markku Leskela

Clean power source utilizing vast logistic fuel reserves (jet fuels, diesel, and coal) would be the main driver in the 21st century for high efficiency. Fuel processors are required to convert these fuels into hydrogen-rich reformate for extended periods in the presence of sulfur, and deliver hydrogen with little or no sulfur to the fuel cell stack. However, the jet and other logistic fuels are invariably sulfur-laden. Sulfur poisons and deactivates the reforming catalyst and therefore, to facilitate continuous uninterrupted operation of logistic fuel processors, robust sulfur-tolerant catalysts ought to be developed. New noble metal-supported ceria-based sulfur-tolerant nanocatalysts were developed and thoroughly characterized. In this paper, the performance of single metal-supported catalysts in the steam-reforming of kerosene, with 260 ppm sulfur is highlighted. It was found that ruthenium-based formulation provided an excellent balance between hydrogen production and stability towards sulfur, while palladium-based catalyst exhibited rapid and steady deactivation due to the highest propensity to sulfur poisoning. The rhodium supported system was found to be most attractive in terms of high hydrogen yield and long-term stability. A mechanistic correlation between the role of the nature of the precious metal and the support for generating clean desulfurized H_2-rich reformate is discussed.

1. Introduction

Our energy infrastructure dictates continued and increased use of fossil fuels for the next several years and maybe decades. The use of domestic resources, such as coal, is especially attractive. Clean power source utilizing vast reserves of other logistic fuels (JP-8, Jet-A, kerosene and diesel) would be the main driver for high efficiency fuel cells. Hydrocarbon fuels such as diesel and jet fuel have logistics (well-established distribution network) and safety advantages for military applications compared to compressed hydrogen. Energy densities of both diesel and jet fuel JP-8 (11.8 and 11.1 kWh/Kg resp.) are much higher compared to lower hydrocarbons (natural gas). Furthermore, Diesel is a petroleum derived product that is a complex mixture of paraffins (n-, iso-, and cycloparaffins) and ring chained aromatic compounds (squaline, tetralin, and methyl naphthalenes). Reforming of diesel to produce hydrogen for solid oxide fuel cells (SOFCs) has great advantages, as the hydrogen density of diesel is very high. The reformate gas contains mainly CO, CO_2, H_2, and trace amount of H_2S. The sulfur products can be removed by sulfur sorbents. A direct application of this technology is by installing SOFC-based auxiliary power unit (APU) in trucks to provide energy instead of relying on running diesel engine. Similarly, fuel cells running on jet fuel reformate are attractive to NASA for its uninhabited aerial vehicle and low emission alternative power missions. The US military has interest in fuel cells due to their lightweight, zero emission and low acoustic signatures in strategic zones. Jet fuels, such as Jet-A and JP-8 are already on board in many applications. If they can be reformed and used in SOFCs military missions can be made more effective. Hydrogen had been touted to be the ideal energy carrier of the future well over a century ago by Verne [1].

However, the infrastructure for fuel cell-based H_2 economy is years or even decades away. Therefore, hydrocarbon

fuels must first be converted into a hydrogen-rich stream. The catalysts used for reforming heavy hydrocarbons are poisoned by sulfur invariably present in logistic fuels as organosulfur, up to 0.3–4% (3000–40,000 wppm) [2]; the level of sulfur in coal varies between 2.3% and 4.5% depending upon the quality of the bituminous coal [3]. During reforming process, this sulfur is also likely to get transformed into H_2S; if not removed effectively, H_2S ($\leq$1 ppm) deactivates the SOFC anode rapidly [4]. Thus, fuel processors are required to convert logistic fuels into hydrogen-rich reformate for extended periods in the presence of sulfur, and deliver hydrogen with little or no sulfur to the fuel cell stack. In order to facilitate continuous uninterrupted operation of logistic fuel processors, robust sulfur-tolerant catalysts ought to be developed.

In the light of the recent quest for cleaner and greener energy, the use of hydrogen-rich reformates of logistic fuels such as Avgas (aviation gasoline), JP-5, JP-8, and Jet-A as the feed for PEMFCs and/or SOFCs for NASA and the Department of Defense, is attractive. Given the energy crisis in the US and especially in Southeast Asia in terms of its ever-rising demand, fuel cells running on clean hydrogen feeds derived from abundant logistic fuels, are attractive options, provided a strategy for effective desulfurization and sustained reforming via robust sulfur-tolerant catalysts is in place.

Much work has been done to better understand the sulfur poisoning of Ni- and Rh-based reforming catalysts [5, 6]. In presence of CeO_2, Ru-supported Al_2O_3 catalyst showed high sulfur resistance in the steam reforming of kerosene [7]; sulfur tolerance increased from 0.1 to 50 ppm. Nevertheless, a highly active sulfur-tolerant catalyst for steam reforming of logistic fuels has not yet been developed.

Even though the key active metals used in the reforming catalysts are Pt, Pd, and Rh, no systematic study exists to compare their performance in the steam reforming of a given logistic fuel under identical experimental conditions. Nor is there a study where the definitive role of one precious metal over the other has been elucidated. Therefore, systematic investigation was undertaken to understand the role of precious metals in imparting sulfur-tolerance to the nanoscale ceria-based reforming catalysts in the process of hydrogen generation via steam reforming. The active metal dispersion in these sulfur-tolerant catalyst formulations was varied between 1 and 1.33 wt.%. The formulations contained either a single precious metal or a bimetallic or a trimetallic combination. These formulations were assessed in terms of their sulfur-tolerance, phase integrity and the quality of reformate from kerosene (JP-8 surrogate) fuel at temperatures typically employed in reforming.

The rationale behind the choice of nanoscale ceria as support material in this work is as follows. While alumina (Al_2O_3) is a common support for a number of catalysts in oil refining due to its high thermal and chemical stability, there a great deal of rationale for using ceria supports in the present work. Ceria is commercially used in catalytic converters as a support for three-way catalyst for reducing harmful emissions from automobiles [8]. It is well known for its high oxygen storage capacity (OSC) and easy reducibility due to its facile $Ce^{III} \leftrightarrow Ce^{IV}$ equilibrium; CeO_2-based materials are quite active and stable both in reducing and oxidizing atmospheres in high-temperature regimes compared to other conventional support systems [9–12]. This, in conjunction with a preparative technique that provides nanoscale particles, results in a high-surface-area catalyst with the possibility of high activity for the reforming of sulfur-laden fuels. When used as a support for precious metal(s), it results in the transfer of oxygen to the supported metals while the support is then reoxidized by the water present in the steam reforming reaction. Increased OSC leads to increase in oxygen vacancies which contribute to increased reducibility of ceria as well. Although, CeO_2 is more active as a reforming catalyst than Ce_2O_3, it can act beneficially towards sulfur tolerance as well, as will be shown later.

Thermodynamically, in a reducing environment Ce_2O_3 has higher sulfidation equilibrium constant than CeO_2, suggesting a possibility of formation of either cerium oxysulfide (partial sulfidation) or cerium sesquisulfide (complete sulfidation). This mechanism might help mitigate sulfur-mediated poisoning and deactivation of ceria-based catalysts in the long run. This sacrificial role may also allow precious metal(s) to remain active longer, resulting in better catalyst life. Furthermore, H_2S adsorption on ceria is partially reversible. The thermodynamics of the CeO_2-H_2S reaction, however, do not allow the reduction of H_2S to below 200 ppm at about 627°C; even at a temperature of 827°C, the H_2S level cannot be reduced to below 100 ppm. This requires ceria to be in a reduced form (CeO_n; $n < 2$) to achieve the removal of sulfur to desired levels. Upon reduction, CeO_2 goes to Ce_2O_3, thereby creating oxygen ion vacancies, and thus sulfidation of ceria occurs rapidly. In the light of these characteristics, ceria was used as a support matrix for the development of sulfur-tolerant catalytic formulations [13–15].

This communication is the first in a series that highlights the performance of single metal-supported nanocatalysts (active metal loading: 1 wt.%) in the steam reforming of kerosene (a JP-8 surrogate) in terms of high ($\geq$75%) hydrogen yield and excellent sulfur-tolerance over extended period of time on stream. A unique feature of these formulations was the unusually low levels of carbon monoxide, carbon dioxide and methane in reformate. A plausible mechanistic correlation between the role of the precious metals and the behavior of the catalyst formulations in terms of the above-mentioned features is also discussed.

2. Experimental Details

Nanoscale support material consisting of 10 mole % gadolinia (Gd_2O_3)-doped CeO_2—hereafter referred to as GDC—was synthesized via ammonia precipitation using appropriate water soluble precursors for cerium and gadolinium (from Alfa-Aesar, MA) followed by hydrothermal treatment of the basic slurry thus obtained, in an autoclave at 240°C, for 2 h. The resulting material was dried overnight and systematic structural and morphological characterizations were carried out to follow the crystallization and phase evolution pathways as a function of calcination temperature-time profile.

The catalysts were formulated by dispersing precious metals onto the GDC support material, using their respective water soluble precursors: ruthenium (III) chloride (99.999%), palladium (II) nitrate (99.95%), and rhodium (III) nitrate hexahydrate (99.999%), all from Alfa-Aesar, MA. For this purpose, aqueous slurry of GDC and the precious metal precursors was homogenized in an evaporator for 4–6 h and the thickened mass was dried overnight in a vacuum oven at 100°C . The dried cake consisting of soft agglomerates was crushed using mortar and pestle, and pulverized in a ball mill using 2-propanol and 5-mm diameter zirconia media. The ball-milled slurry was dried again under ambient conditions and sieved through 325 mesh screen. Each formulation was calcined in air at 700°C for 2 h. These formulations contain, on metal weight basis, 1% of Ru (ruthenium), Pd (palladium) and (Rh) rhodium each and will be referred to as such.

The catalysts were characterized by a host of techniques with respect to their crystallinity, active metal dispersion, structural and morphological features. Temperature programmed reduction (TPR) of the as-prepared reforming catalysts was conducted using the Micromeritics AutoChem 2910 (Norcross, GA). TPR analysis was used to identify reduction temperatures of the noble metal active sites in the catalyst as well as their hydrogen uptake volume. This technique was used to optimize a systematic activation protocol for each catalyst prior to sulfidation and reforming experiments.

Independent sulfidation experiments were carried out by introducing 1000 ppm H_2S-balance nitrogen stream over a bed of 1 g of powder catalyst at 800°C for 4 and 24 h. X-ray powder diffraction (XRD) signatures on the as-prepared and the postsulfided sample were collected on a Philips diffractometer (PW 3050/60 X'pert Pro), using monochromatic CuKα_1 radiations ($\lambda = 1.54056\,\text{Å}$) and Ni filter. The total amount of sulfur retained by the catalysts was quantified by wet chemical techniques by NSL Analytical, Cleveland, OH.

Steam-reforming experiments were carried out on powder samples (1 g) using kerosene as the fuel. LECO test established the sulfur content of this kerosene sample to be 260 ppm as determined by Paragon Laboratories, MI. The packed-bed reactor used here was a quartz tube, 19-in long and 1-in diameter. The catalyst was packed in a stainless steel filter with 5 μm size pore from Swagelok. The filter containing the catalyst was placed in the center of the reactor and plugged with loosely packed quartz wool. The quartz reactor was then placed in a 1-in. ID split tube furnace equipped with a PID controller.

Water and fuel (kerosene) were pumped into the reactor with high precision HPLC pumps. Argon was used as a sweep gas for the reforming reaction. The steam to carbon ratio (S/C) was maintained at 3. The flow rates of water and fuel were adjusted to maintain a constant space velocity in the reactor at $65,000\,\text{h}^{-1}$. The feed stream containing sweep gas, water, and fuel was first introduced into a preheater (vaporizer furnace) operated at 250°C to ensure complete vaporization of the feed. All reforming reactions were carried out at 800°C. The product stream coming out of the reactor was drawn into a condenser to separate the liquid and gas products. The liquid fraction consisted mainly of water and unreacted fuel with traces of other liquid hydrocarbons. The composition of the gas reformate mixture was analyzed via Gas Chromatograph (GC). Shimadzu GC, Model 2010 equipped with pulsed discharge helium ionization detector (PDHID) and flame photometric detector (FPD) was used to analyze the gas products. The FPD on the GC was facile in detecting sulfur species in the reformate stream. The duration of the experiment was determined by the stability and activity exhibited by the catalysts on stream. The hydrogen yield was defined as

$$\%\text{yield} = \frac{(F_i)}{(v_i)\cdot\left(F_{j,0}\right)} * 100, \tag{1}$$

where F_i is the moles of species i produced per min, v_i is the stoichiometric coefficient of species i, and $F_{j,0}$ is the molar flow rate of the reactant in moles/min.

The reforming tests were conducted over extended period of time and terminated as per a predetermined criterion of arbitrarily selected hydrogen yield reducing to 20% of its highest level or the sulfur level reaching 50 ppm (as H_2S) in the exit stream. Concentration of other gases was also monitored simultaneously as a function of time. The GC was calibrated with respect to hydrogen, carbon monoxide, carbon dioxide, and methane—the major constituents in a typical reformate—over a wide range of concentrations. GC was also calibrated with respect to H_2S concentration between zero and 1000 ppm.

Systematic microstructural analysis was performed by scanning electron microscopy (SEM-Phillips XL 30 FEG) and transmission electron microscopy (TEM-JEOL 3011). Both these techniques are equipped with the capability of performing energy dispersive X-ray spectroscopy (EDS) as well. The SEM is equipped with Rutherford's back scattering electron mapping (RBSE) as well. The chemical state analysis of the active components in the postreformed samples was performed by using X-ray Photoelectron Spectroscopy on the Kratos Axis Ultra XPS.

3. Results and Discussion

3.1. Structural and Microstructural Artifacts of the Precious Metal-Supported Nanocatalysts. The morphological features of the as-prepared catalysts are shown in the TEM images of Figure 1; clearly all formulations possess nanofeatures. The contrasting light and dark particle contours in these images belong to the GDC support and the noble metals, respectively. This further suggests that despite low concentration, the dispersion of the catalytic metals is highly uniform throughout the matrix. Thus, the preparatory technique utilized for making them is quite effective in yielding uniform distribution of the precious metals throughout the support. The nanofeatures observed in the TEM images are also corroborated by the rather broad diffraction peaks in the XRD patterns of the powders calcined at 700°C for 2 h, shown in Figure 2.

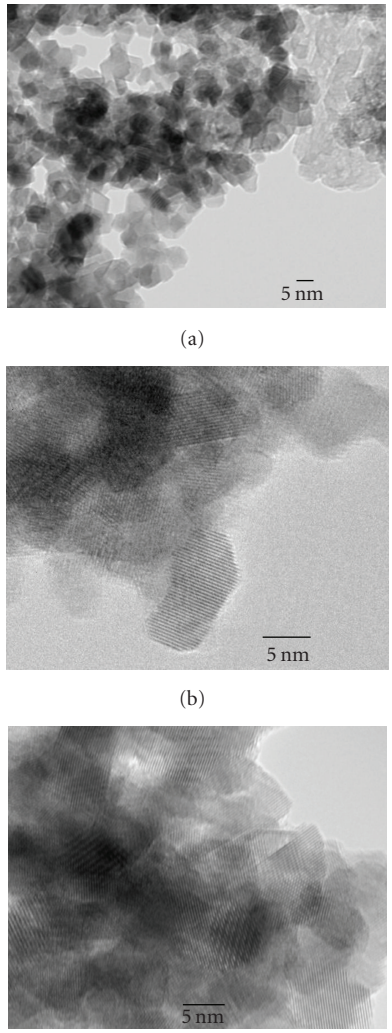

Figure 1: TEM images of 1 wt% Ru (a), Pd (b), and Rh (c), supported GDC matrices. Scale bar: 5 nm.

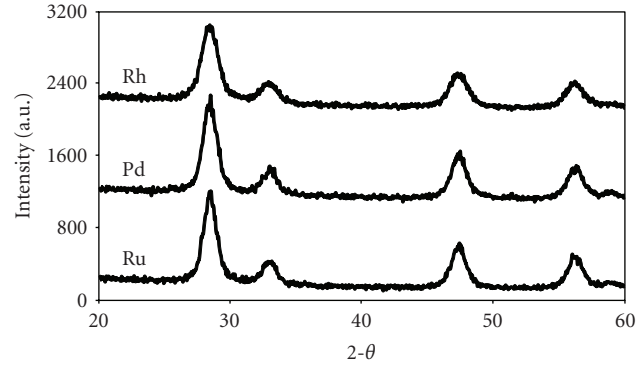

Figure 2: XRD signatures of virgin monometal supported catalysts (calcined: 700°C/2 h).

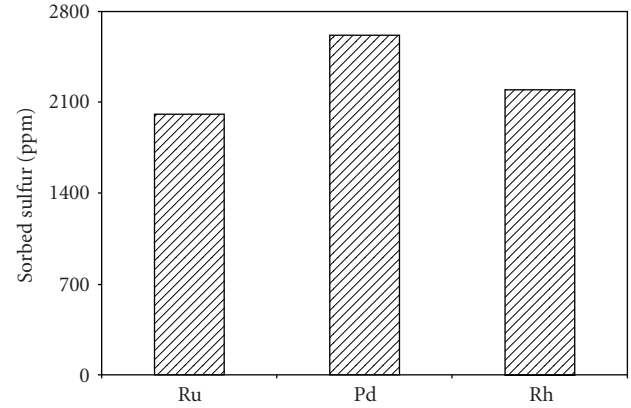

Figure 3: Quantification of sulfur pick-up by the formulations developed in this work.

The gross XRD patterns are typical of those for 10 mole% gadolina-doped ceria (GDC) used in this work [16]. Peaks for the precious meals are not discernable due to their low loading (1 wt.%), which is below the detection limit of the XRD technique. Estimation of the crystallite size using Scherrer's equation, yielded values between 5 and 7 nm, which is in excellent agreement with those seen in the TEM images. The nanofeatures of these formulations ensure large surface area and effective noble metal dispersion. This lowers the loading and keeps the manufacturing cost low without compromising the performance.

3.2. Propensity to Sulfur Tolerance. With logistic fuels, sulfur tolerance of the reforming catalyst is of prime importance, as recent studies have shown irreversible sulfur poisoning to be the main cause of their deactivation [4]. Thus, it is imperative that the catalysts intended for the reforming of sulfur-laden fuels be evaluated for their sulfur tolerance first. Therefore, the catalysts synthesized in this work were first examined for their sulfur tolerance and phase integrity under conditions of sulfur exposures for extended period at the temperature employed for reforming (800°C). Packed beds of the catalyst powders (1 g) were exposed to stream containing 1000 ppm H_2S in nitrogen for 4 and 24 h, and the postsulfided samples were analyzed for sulfur pick-up. The results of 24 h soak are presented in Figure 3.

The amount of sulfur sorbed by these formulations showed an interesting pattern. First, as expected, it is proportional to the soak-time. Second, in terms of the precious metal, the sulfidation susceptibility follows the pattern: Ru < Rh < Pd. This, in terms of reforming of a sulfur-laden fuel, means that the highest and the lowest sulfur-tolerance would be exhibited by Ru- and Pd-supported formulations, respectively. This prediction would be evaluated in the light of steam-reforming data reported later in the paper.

Figure 4 shows the TEM images of the postsulfided catalysts while their XRD patterns are shown in Figure 5.

Clearly, there is evidence of grain growth in the samples sulfided for longer (24 h) duration; the particles have grown to about 10–12 nm in size, a fact which is corroborated by the peak narrowing seen in the XRD signatures. The peak sharpening is an indication of systematic crystallinity enhancement as a function of time at high temperature.

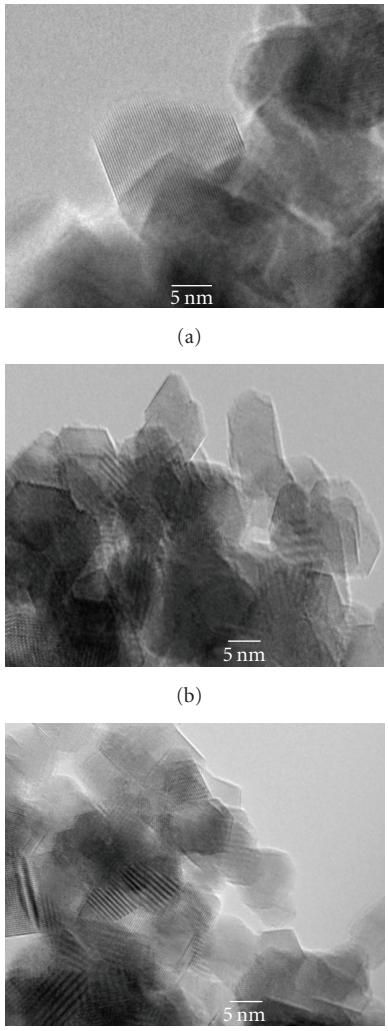

Figure 4: TEM images of sulfided Ru (a), Pd (b), and Rh (c); bar: 5 nm.

In this case, the peak narrowing is an artifact of grain growth and crystallite size enhancement upon sulfidation. However, the crystallite texture is maintained; the crystallite size calculation and TEM images suggest that the grain growth in the sulfided samples is only nominal, indicating no significant surface area reduction occurred. It can also be seen that no new phases could be discerned, suggesting phase integrity was preserved under sulfidation at high temperatures. Moreover, the TEM images indicate some agglomeration as well, upon sulfidation. The obvious question is: does this grain growth and agglomeration adversely affect the reforming performance of these catalysts? The answer is no, as will be seen from the data reported in the following section.

3.3. Steam-Reforming Characteristics. As stated previously, all kerosene steam-reforming experiments were carried out at 800°C and atmospheric pressure (~14.7 psi) keeping the steam to carbon ratio constant at 3.0. The experiments were

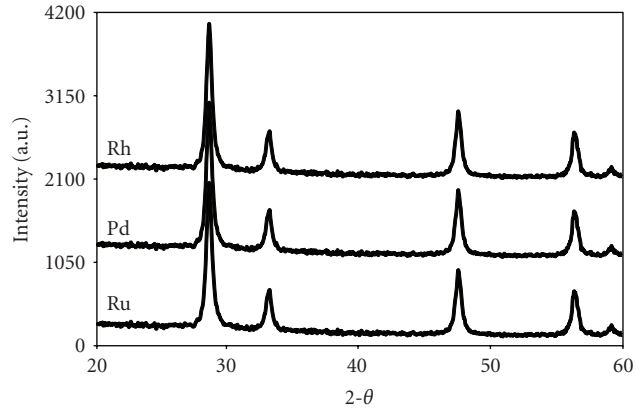

Figure 5: XRD patterns of the catalysts sulfided for 24 h at 800°C in 1000 ppm H_2S/bal. N_2.

Table 1: Performance summary of the monometal-supported reforming catalysts.

	Ru	Pd	Rh
Max. H_2 yield (%)	79	84.4	87
Duration (h) of steady level H_2 yield	51	—	55
Time (h) to deactivate to 20% H_2 yield	66	59	68

terminated when the hydrogen yield reached about 20% or the sulfur (as H_2S) peaked to about 50 ppm in the reformate. Figure 6 compares the reformate compositions resulting from the steam reforming of kerosene on three monometal supported reforming catalysts, as a function of time on-stream.

The performance trend in term of hydrogen yield in these catalysts is characteristic of the precious metal on them, as seen from the data summarized in Table 1.

Since the exact composition of the fuel (kerosene) is not precisely known, thermodynamic calculations were conducted on a close surrogate, which comprised of a mixture of 70% n-hexadecane and 30% toluene. This choice was based on similar assumptions used by others in the literature [17]. Equilibrium conversions were estimated by Invensys Pro/II Simulation Software Version 8.3 [18, 19]. The conditions chosen for simulation were identical to those employed in the reforming experiments: $T = 800°C$, $P = 1$ atm, molar feed ratio of S/C = 3 and GHSV of $65,000\,h^{-1}$. Assuming complete conversion of the fuel, the equilibrium concentrations thus obtained for H_2, CO, CO_2, and CH_4 were 78.34, 9.86, 11.27 and 0.53%, respectively. These simulation results are similar to those reported in the literature for n-hexadecane reforming [18, 20]. As can be seen, the reformate composition shown for the three calayst systems in Figure 6 are in good agreement with the equilibrium data obtained from simulation. The hydrogen content in the reformate stream was slightly lower than the equilibrium conversion. It may be recalled that traces of unreacted liquid fuel was seen in the condensate. This clearly suggests that fuel conversion was not complete

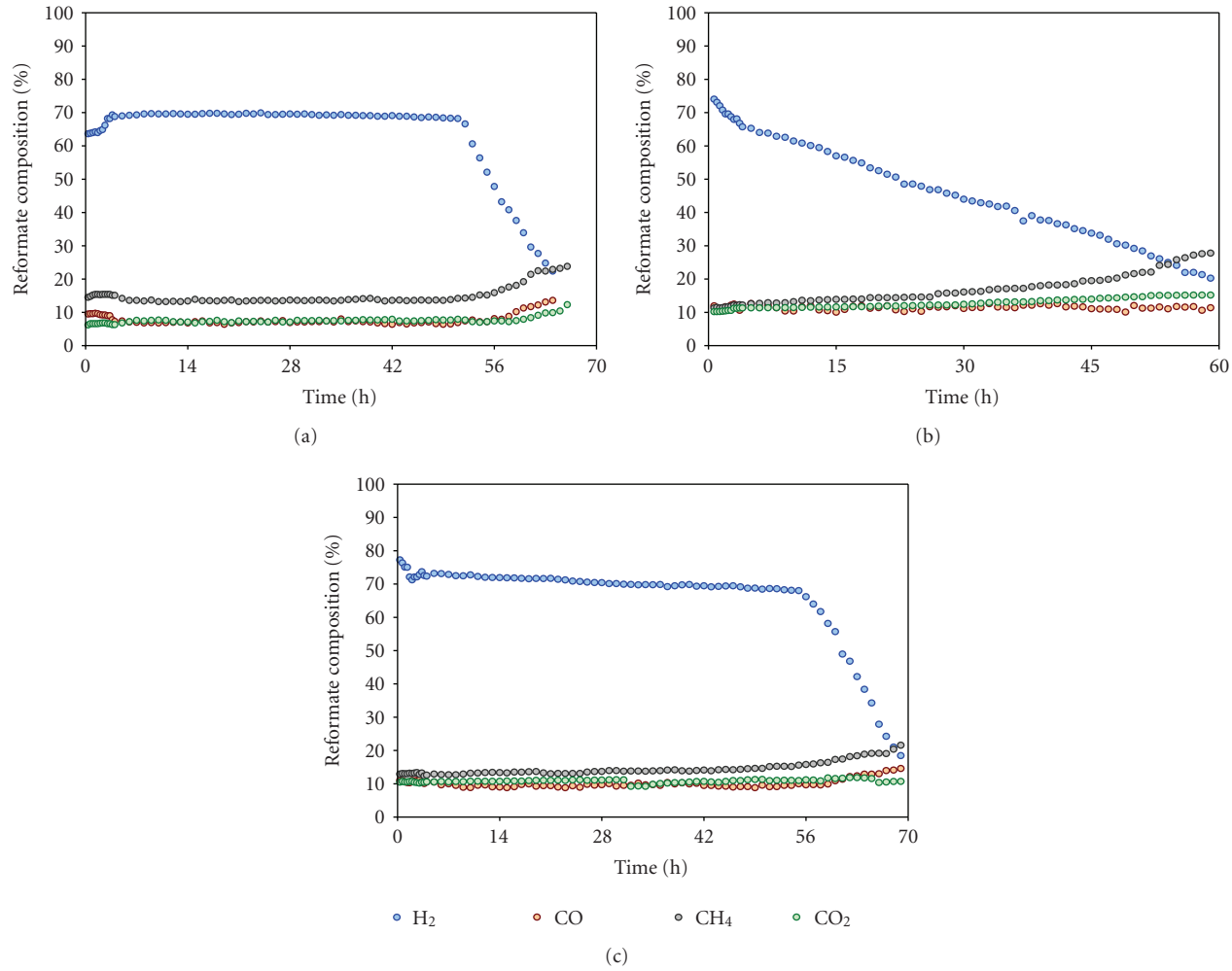

Figure 6: Composition of kerosene reformates using: (a) Ru, (b) Pd, and (c) Rh.

as presumed in the thermodynamic calculations by the simulation technique.

Since kerosene contains 260 ppm of sulfur, it is imperative to understand the difference in performance of these catalysts in terms of their behavior towards sulfur as well. For that purpose, the sulfur level (as H_2S) in the exit stream was also monitored whose concentration as a function of the progress of the reaction is shown in Figure 7.

Several interesting aspects emerge. First, the steady-state hydrogen concentration in the reformate is ~70% in all but one case (viz., Pd-based catalyst) and stays that way for more than 50 h continuously. The Pd-based catalyst appears to deactivate quickly from the very beginning of the reforming process, as evidenced by the steadily declining level of hydrogen in the reformate, suggesting that in the case of Pd-supported GDC, the catalyst poisoning had begun very early on. The sulfur level in the exit drops to 2.03 ppm at the end of 11 h on-stream, beyond which it shows steady increase with a concomitant decline in hydrogen concentration. The characteristic "tilted L-shaped" locus of sulfur concentration with time is indicative of rapid and quantitative sulfur-poisoning of Pd-based catalyst. In the light of Figure 3, it can be inferred that the formation of thermodynamically stable PdS phase began from the very start. Therefore, at the first glance, it would appear that Pd-supported formulation is not a preferred reforming catalyst for a logistic fuel such as kerosene sulfur-laden to the extent of 260 ppm sulfur.

Nevertheless, the Pd-supported catalyst still continues to generate hydrogen at a reasonable albeit steadily diminishing rate. The distinct difference in slope seen in Figure 6(b) for hydrogen concentration is likely due to two somewhat different deactivation mechanisms. It is evident that the initial far quicker surface-dominated deactivation is followed by bulk sulfidation of the active metal in the later stages. The latter is diffusion-controlled and hence somewhat slower; at a given temperature (800°C in this case) it would have a finite value of the limiting rate constant.

Therefore, as seen from Figure 8, the rather high (>84%) hydrogen yield calculated as per (1), in the early stage of steam reforming is due to the exceptionally high activity of the fresh Pd-supported catalyst. However, after about 4 h on-stream, it is believed that the surface sulfidation of palladium (hence more rapid decline in the yield) is completed and changes to bulk sulfidation (diffusion controlled). Thus, for

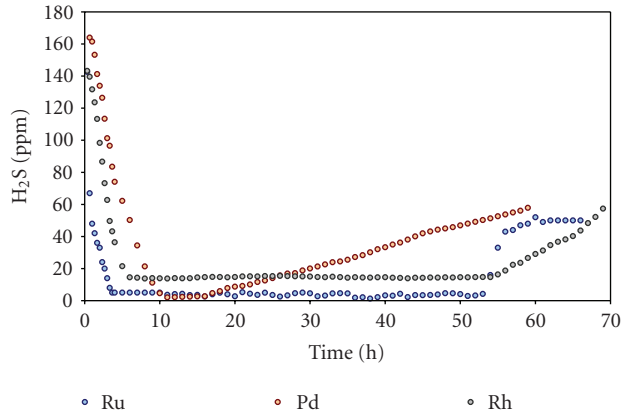

FIGURE 7: Trend in H_2S concentration build-up in the exit stream with time on-stream.

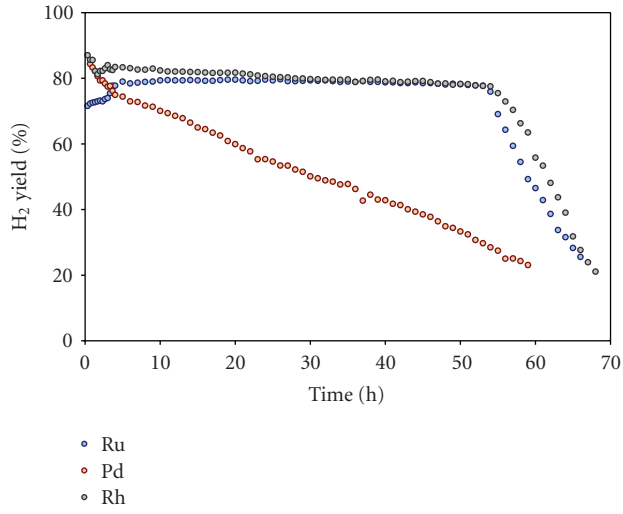

FIGURE 8: Comparison of hydrogen yield in kerosene reformates using different catalysts.

the remainder of the duration on-stream, the deactivation becomes more monotonic.

In contrast, the performance of the Ru- and Rh-based catalysts is superior, both in terms of hydrogen yield and on-stream stability over extended period. The steady-state hydrogen yield is about 80% or higher for about 51–55 h in both the cases. It takes another 15 h for the amount of hydrogen to fall below the predetermined level of 20%. A comparison between Figures 7 and 8 brings out an interesting correlation between hydrogen and sulfur level in the kerosene reformate. The initial 3–5 h on-stream represent unsteady-state during which the sulfur level drops precipitously and then attains a low value which remains unaltered for about 50 h. This trend is reflected in the fluctuating hydrogen yield in the initial period, followed by a corresponding flat region for the next 50 h or so, marking the attainment of steady-state with respect to hydrogen generation as well.

In the light of Figures 7 and 8, certain distinct behavioral features of Ru and Rh-based catalysts become evident. For example, in the case of Ru-supported GDC, the hydrogen production in the early stages of reforming is somewhat lower (~71.5%) which increases to about 79% once the catalyst stabilizes and steady-state is achieved. This is in direct correspondence to the drastic drop in sulfur level during the first few hours, leveling off to about 3 ppm H_2S (kerosene originally contains 260 ppm sulfur) for the remainder of the steady-state duration. A similar trend is seen in the case of Rh-supported GDC. However, in this case, the hydrogen level drops from ~87% in the early part of reforming to about 79% in the stead-state regime. Correspondingly, sulfur in the reformate levels off around 15 ppm. In both the cases, the decline in hydrogen yield beyond 54 h on-stream signals the catalytic deactivation which is corroborated by the concomitant increase in sulfur level in the reformate. With regard to steady-state hydrogen yield, the reformation capability of Ru- and Rh-based catalysts is almost identical. However, their sulfur-tolerance characteristics are different. In the case of Pd-supported catalyst, the quicker reduction and attainment of lower amount of residual sulfur in the reformate indicate better reforming capability together with superior sulfur tolerance. Moreover, as the hydrogen yield begins to decline probably due to sulfur-poisoning, the sulfur concentration in the exit stream increases rapidly and attains a new steady-state value of 50 ppm H_2S. This is in contrast to Rh-based where the steady-state sulfur concentration in the reformate is somewhat higher (~15 ppm) than in Ru-based (~3 ppm) and increases steadily, once the catalyst deactivation has set in. Thus, Ru-based formulation appears to be more sulfur-tolerant than the Rh-based analog in the case of kerosene reforming.

This distinctive behavior of these formulations with regard to their tolerance to sulfur in a real logistic fuel such as kerosene has been observed perhaps for the first time. This prompts us to suggest the following phenomenological mechanism operative in the two cases.

In early stages, the hydrogen produced during steam-reforming acts as a hydrodesulfurization (HDS) precursor converting the organosulfur into H_2S [21–23].

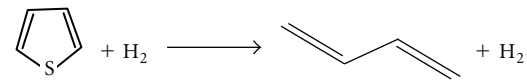

Thiophene is used in the above example for illustrative purpose. Credence to this mechanism is derived from Figure 7, where H_2S is detected from the very beginning of the reaction.

The hydrogen sulfide thus formed then partially reacts with nanoscale precious metals. In the case of palladium, the following reaction can be envisaged.

$$\mathrm{Pd} + \mathrm{H_2S} \longrightarrow \mathrm{PdS} + \mathrm{H_2}. \quad (2)$$

In the case of ruthenium, it binds sulfur as ruthenium sulfide, RuS_x [24]:

$$\mathrm{Ru} + x\mathrm{H_2S} \longrightarrow \mathrm{RuS}_x + x\mathrm{H_2}. \quad (3)$$

In the case of Ru-supported GDC catalyst, the sulfidation could be viewed as a two-stage process, accounting for

the two steady-states observed in Figure 7. Ruthenium compounds exhibit at least eight oxidation states, but the +2, +3, and +4 are the most common. One would expect these to be the most prevalent ones under conditions existing in reforming.

One could anticipate the occurrence of one or all of the following reactions.

$$\mathrm{Ru} + \mathrm{H_2S} \longrightarrow \mathrm{RuS} + \mathrm{H_2}, \tag{4a}$$

$$3\mathrm{RuS} \longrightarrow \mathrm{Ru_2S_3} + \mathrm{Ru}, \tag{4b}$$

$$\mathrm{Ru} + 2\mathrm{H_2S} \longrightarrow \mathrm{RuS_2} + 2\mathrm{H_2}, \tag{4c}$$

$$2\mathrm{Ru} + 3\mathrm{H_2S} \longrightarrow \mathrm{Ru_2S_3} + 3\mathrm{H_2}, \tag{4d}$$

$$2\mathrm{RuS} \longrightarrow \mathrm{RuS_2} + \mathrm{Ru}, \tag{4e}$$

$$\mathrm{Ru_2S_3} + \mathrm{H_2S} \longrightarrow 2\mathrm{RuS_2} + \mathrm{H_2}. \tag{4f}$$

The transition of the atomic ratio of ruthenium to sulfur from 1 : 1 (in RuS) to 1 : 1.5 (in Ru_2S_3) to 1 : 2 (in RuS_2) as outlined in the above scheme is substantiated by the observation made by Pecoraro and Chianelli [22] that the sulfides of ruthenium exhibit exceptional HDS activity. A similar conclusion was arrived at by Ishiguro et al. [25] who examined the evolution of ruthenium sulfide nanoclusters on titania support.

On the other hand, as can be seen from Figure 7, the drop in sulfur concentration in the case of Rh-supported GDC catalyst is somewhat slower (~6 h) compared to ~3 h in the case of Ru-supported GDC catalyst. This could be ascribed to the single-step process, where the most stable rhodium sulfide, Rh_2S_3 is partially formed [26].

$$2\mathrm{Rh} + 3\mathrm{H_2S} \longrightarrow \mathrm{Rh_2S_3} + 3\mathrm{H_2}. \tag{5}$$

At this juncture it is relevant to ask the question: is the sulfidation of the precious metals as outlined above feasible as the key mechanism, responsible for the observed sulfur tolerance? The answer is no; while this scheme is feasible, it cannot possibly be the primary mechanism. Were this true, the sustained high hydrogen yields over long period as recorded in Figure 8 would not be possible. It stands to reason that the outstanding performance of the formulations developed in this work is borne out of the fact that there is another mechanism for sulfur resistance.

It is well-known that ceria itself is capable of forming an oxysulfide [27–30]. Therefore, in reducing environments, due cognizance should be given to the highly favorable thermodynamics of CeO_2-H_2-H_2S system.

$$\mathrm{CeO_2(s)} + (2-\mathrm{n})\mathrm{H_2(g)} \longrightarrow \mathrm{CeO_n(s)} + (2-\mathrm{n})\mathrm{H_2O(g)}, \tag{6a}$$

$$\mathrm{CeO_n(s)} + \mathrm{H_2S(g)} + (2\mathrm{n}-3)\mathrm{H_2(g)} \longrightarrow \mathrm{Ce_2O_2S(s)} + 2(\mathrm{n}-1)\mathrm{H_2O(g)}. \tag{6b}$$

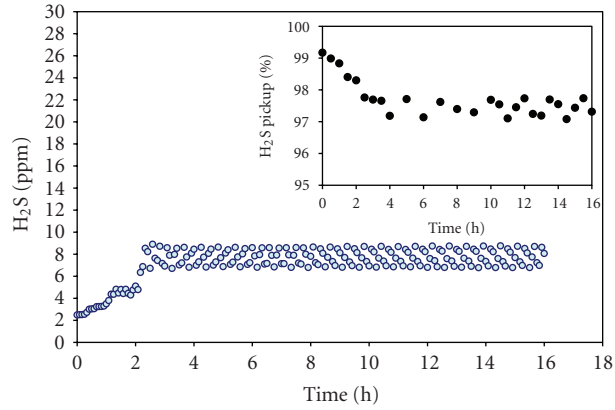

Figure 9: Evidence of sulfur pick-up propensity of pure GDC at 800°C.

To clarify the debate whether this is happening in our case where the precious metals are supported on ceria matrix, an independent sulfidation experiment on GDC alone was performed using a stream of 90% H_2, 9.97% N_2 and 300 ppm H_2S at 800°C for 16 h, simulating the reducing conditions and sulfur level prevailing in the case of original fuel (kerosene). The time dependence of the sulfur level in the exit stream is shown in Figure 9; the extent of sulfur picked up by GDC during the same period is shown in the inset.

As can be seen clearly, sulfur scavenging appears to be almost 100% from the very beginning of the simulated reaction, reaches steady-state rather quickly and its concentration in the exit stream hovers around 8 ± 1 ppm for the next 14 h. This unequivocally establishes that the primary sulfur tolerance in the steam reforming of kerosene comes from the inherent and thermodynamically feasible sulfurizability of the ceria support matrix; by virtue of this the noble metals are spared sulfur attack and remain active in the reforming of the sulfur denuded fuel leading to high hydrogen yield.

At this juncture, it is worth pointing that the most extensively employed inert catalytic support, viz., alumina (γ or α) is not endowed with such unique capability, which explains the short-term activity of such catalysts, even those which have far higher loading of noble metals [31–33]. In the present case, the only exception appears to be the Pd-supported formulation, where it seems that the along with ceria, the precious metal also experienced preferential sulfur ingress leading to monotonic deactivation of the catalyst from the very beginning of the process.

TEM images collected on the postreformation catalysts are shown in Figures 10 and 11.

The crystallite size calculations and TEM images suggest grain growth. However, the size of GDC grains in the postreformed samples was between 8–12 nm which suggests that the grain growth is very nominal. Furthermore, it can be clearly seen from the images that in spite of grain growth, the dispersion of the noble metals through the matrix remained uniform. The dispersion of the respective noble metal is marked clearly on the images. As it was

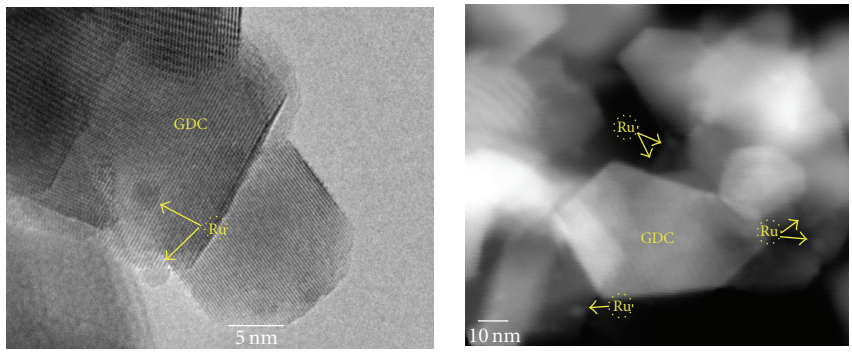

(a) (b)

Figure 10: High resolution (a) and scanning mode (b) TEM images of the postreformed Ru-GDC catalyst; individual noble metal particles (~2 nm) are clearly visible.

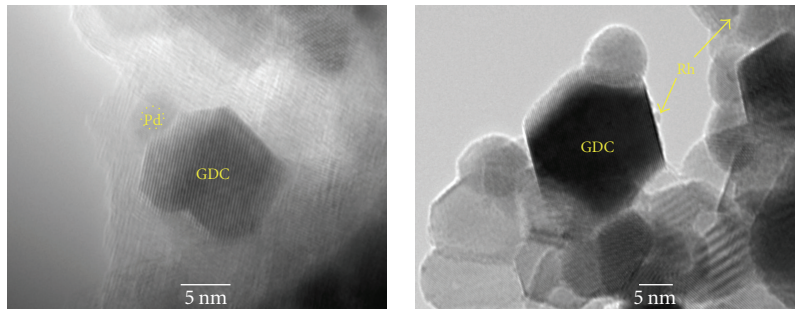

(a) (b)

Figure 11: TEM images of the postreformed Pd-based (a) and Rh-based (b) catalyst.

stated earlier, GDC offers several advantages over traditional support materials (such as γ-Al_2O_3); structural integrity and sintering resistance are definitely the salient features. The EDS analyses (not shown here) did not give any evidence of carbon deposition either.

Systematic XPS characterization was carried out on the as-prepared and sulfided GDC samples and the results are shown in Figure 12.

The XPS investigation indicates that the Ce^{3+} and Ce^{4+} species can be differentiated with distinct line shapes corresponding to various final states. As can be readily seen from this figure, the intensity of the peaks around ~914, 905, 897, 890, and 884 eV in the as-prepared sample, which correspond to Ce^{4+} oxidation state, decreased and those around ~886 and 880 eV in the sulfided samples increased; the later correspond to Ce in 3+ oxidation state. This implies that in the sulfided sample, both Ce^{4+} and Ce^{3+} oxidation states coexist. The slight shifts seen in the peak positions of the virgin and the sulfided samples could be ascribed to difference in the local atomic environment of Ce in the gadolinia doped-ceria (GDC) as opposed to pure ceria (CeO_2), on which the XPS data are generally acquired and/or reported [34–36].

X-ray photoelectron spectra were also collected on the respective monometal-supported catalysts after steam reforming of kerosene, and are presented in Figure 13. The

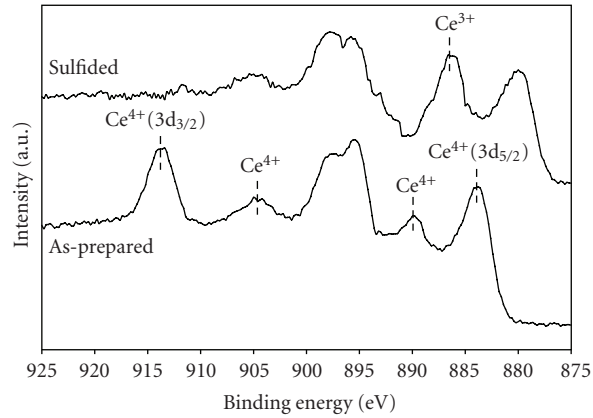

Figure 12: Comparison of the XPS signature of virgin GDC sample with that sulfided at 800°C for 16 h in a gas stream containing 300 ppm H_2S.

XPS peak in Figure 13(a) at 284 eV corresponds to Ru($3d_{3/2}$) in 4+ oxidation state [37]. No peak at 280 eV corresponding to Ru($3d_{5/2}$) in metallic state is present [37], suggesting that the noble metal did not undergo reduction to zerovalent elemental Ru during reformation of kerosene. Peaks at 336 and 342 eV in Figure 13(b) belong to $Pd_{5/2}$ and $Pd_{3/2}$,

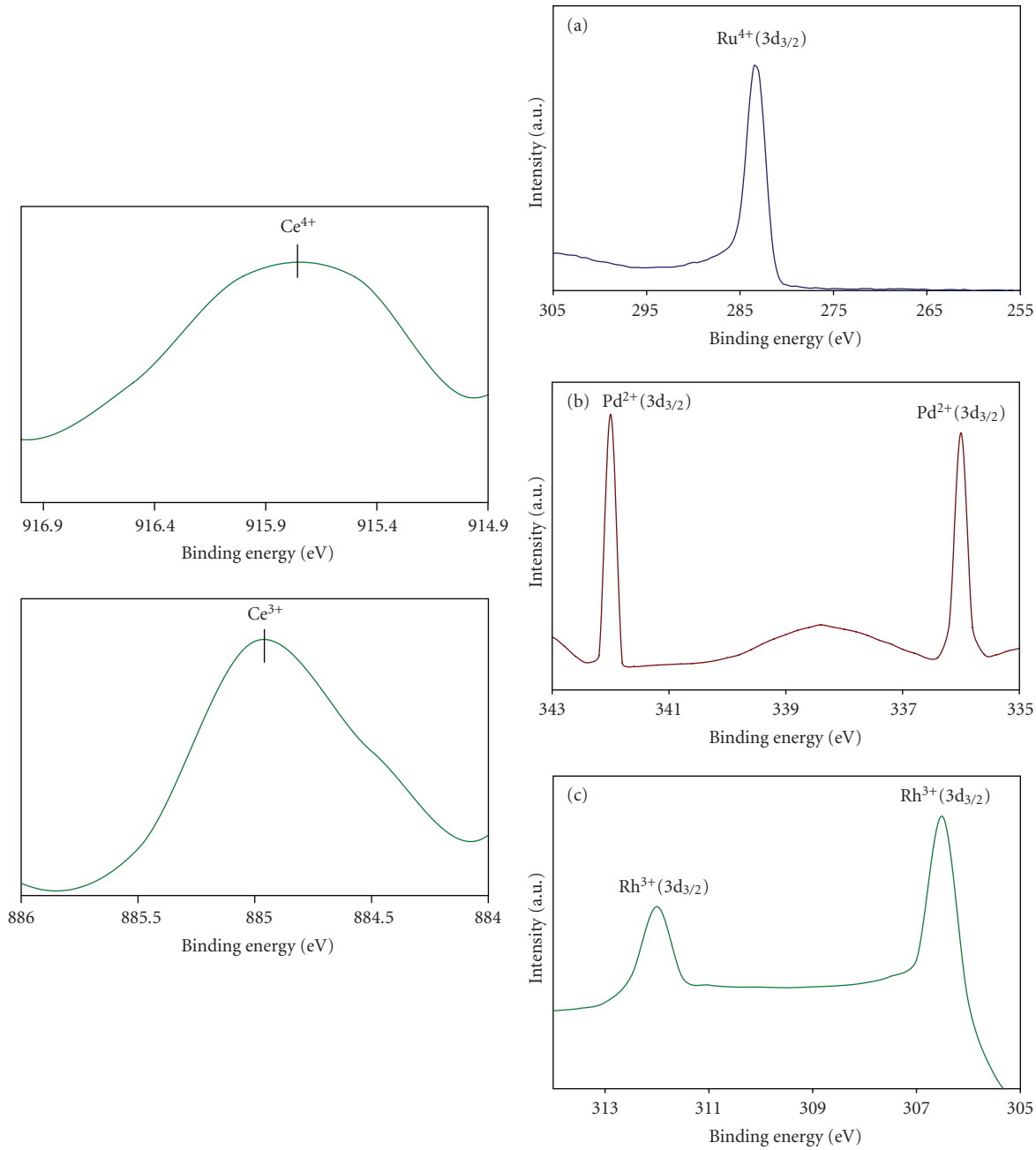

Figure 13: Characteristics XPS signatures of the precious metals in the postreformation catalysts; those for Ce(3d) seen in various oxidation states are also included.

respectively [38], indicating that Pd in the postreformed catalyst is in Pd (II) oxidation state. Similarly, the final oxidation state of rhodium in Rh-based sample is 3+, denoted by two peaks at 306.4 and 312 eV corresponding to Rh ($3d_{5/2}$) and Rh ($3d_{3/2}$), respectively [39].

These spectroscopic and microscopic data provide unequivocal evidence that the ceria support does participate in sulfur uptake from the fuel, thereby allowing the precious metals in Ru- and Rh-supported fromulations to perform actively as the fuel reforming component. The increase in sulfur level in the exit stream and the decline in hydrogen yield the at the end of steady-state regime, seen in Figures 7 and 8, respectively, marks the eventual sulfidation of the respective precious metal in the three catalyst formulations, employed in this work.

Based on these self-supporting experimental evidences, a phenomenological mechanism operative in the steam-reforming of a sulfur-laden logistic fuel (such as kerosene, used in this case) on monometallic catalysts, emerges. The mechanism essentially involves a sequential combination of the reactions shown in (2) through (6a)-(6b), and can be summarized as follows.

As stated earlier, all the catalysts were made active by a prior hydrogen reduction step at 450°C for 1 h. This pre-reforming protocol renders the precious metals active by reducing them to their elemental state. It was also observed that hydrogen is produced in rather high concentration from the very beginning of fuel reforming. Under these conditions, it is correct to envisage the reduction of stoichiometric ceria (CeO_2) to CeO_n ($n < 2$) as per (6a). Reduced ceria is more susceptible to sulfidation than its stoichiometric analog.

Therefore, the initial drastic drop in the H_2S level comes from the sulfidation of reduced cerium oxide in the catalyst via (6b).

It is also not incorrect to assume that in such a reducing environment, the organosulfur species in the fuel are degraded and form H_2S.

The approach of a thermodynamic equilibrium in the CeO_n-H_2S-Ce_2O_2S phase field coincides with the arrival of the kinetic steady-state, which signals the on-set of a period of steady hydrogen generation, during which both H_2 and H_2S level in the exit stream remain practically constant. It is hypothesized that during this period, sulfur pick-up by the noble metal(s) occurs at steady albeit rather small rate, without significantly affecting the reforming propensity of the catalyst as a whole.

When the noble metal supported on ceria matrix also get completely sulfided, deactivation begins to set in. This is marked by the drop in hydrogen level and increase of sulfur levels in the stream at the end of steady-state. It should be emphasized that ceria by itself is not a reforming catalyst. Therefore, as soon as the active metal is poisoned by sulfide phase formation, the reforming capability of the catalyst plummets. This general scheme is reflected in the sequence shown in Figure 14.

However, as seen in the case of Pd-based system, there was no steady hydrogen production period. We explained it in the light of its highest sulfur pick-up, showing that compared to Ru and/or Rh, Pd has very high sulfur affinity. Therefore, in this case, it is believed that Pd begins to sulfide competitively along with the reduced ceria, from the very onset of reforming thereby causing immediate and steady catalyst deactivation.

The proposed mechanism is in total agreement with the observed behavior in the sulfidation as well as reforming experiments over extended periods of time. It explains the role of each of the noble metals in the reforming of sulfur-laden fuels.

3.4. Mechanism of Formation of Lower Fractions of Carbonaceous Species in the Reformate. Yet another unique feature seen in the steam reforming of kerosene with monometal-supported ceria catalysts in addition to exceptionally high hydrogen yield, is the unusually higher level of methane in the dehumidified reformate. Depending up on the nature of fuel, the typical constitution of the steam reformed reformate varies widely. In the case of natural gas, it comprises about 46% H_2, 7–10% CO, 6% CO_2, 2-3% CH_4 and 1% N_2 with balance water, while the average composition of coal syngas is about 29% H_2, 29% CO, 12% CO_2, and 3% N_2 with balance water [40]. As can be seen from Figure 6, the steam-reformed kerosene reformates contain, on an average, about 9-10% CO, 9-10% CO_2 and 14-15% CH_4, in the flat (steady-state) regime. Once the catalyst degradation attended by a decline in hydrogen ensues, there is a slight upward trend in the concentration of CO, CO_2 and CH_4 as well. However the equilibrium conversion data calculated by simulation and reported above predicts the theoretical methane content in the reformate stream to be only 0.53%. A space velocity of $65,000\,h^{-1}$ was used in these experiments. Also the presence of small level of unreformed fuel in the condensate was detected. Hence, it is possible that incomplete conversion of the fuel at such a high space velocity yielded higher methane content in the reformate.

On the other hand, the higher level of methane in the reformate could be explained if one assumes that the catalysts used in this work are also capable of in-situ methantion of carbon monoxide and carbon dioxide in the presence of hydrogen. This would explain the lower level of carbon monoxide and carbon dioxide, and higher fraction of methane.

The possible pathways for the methanation reactions could be written as

$$4H_2 + CO_2 \longrightarrow CH_4 + 2H_2O \qquad \Delta G^o_{1073K} = -68.4\,\text{kJ}\,(\text{mol}\,CO_2)^{-1}, \tag{7a}$$

$$3H_2 + CO \longrightarrow CH_4 + H_2O \qquad \Delta G^o_{1073K} = -21.4\,\text{kJ}\,(\text{mol}\,CO)^{-1}, \tag{7b}$$

$$7H_2 + CO + CO_2 \longrightarrow 2CH_4 + 3H_2O, \qquad \Delta G^o_{1073K} = -89.8\,(\text{mol}\,[CO, CO_2])^{-1}. \tag{7c}$$

As could be seen, all these reactions are thermodynamically favored. In order to verify their practical feasibility, independent experiments were carried out under the conditions of catalytic reforming of kerosene in the same reactor at 800°C and atmospheric pressure, without steam, using the formulations developed in this work. The molar ratios of $CO_2 : H_2$, $CO : H_2$, and $CO : CO_2 : H_2$ in the gaseous mixtures were maintained at 1 : 4, 1 : 3 and 1 : 1 : 7, respectively, as per the stoichiometry shown in (7a)–(7c).

In order to gauge the propensity of the catalyst to the change in composition and content of the mixture, the reactive components were varied while the reaction was in progress. For example, after flowing a stoichiometric mixture of CO_2+H_2 (7a) for the first 4 h, it was switched to the CO+H_2 mixture (7b) for the next 4 h and finally to CO+CO_2+H_2 mixture (7c) for the next 16 h. Composition of the mixture was continuously monitored during the experiment, by letting the exit stream after water removal via condensation into the GC. The results are shown in Figures 15(a)–15(c).

By applying thermodynamic considerations to the steady-state kinetics at 800°C and atmospheric pressure (101.325 kPa), we could compute the theoretical equilibrium concentration of the species in these mixtures [41], as

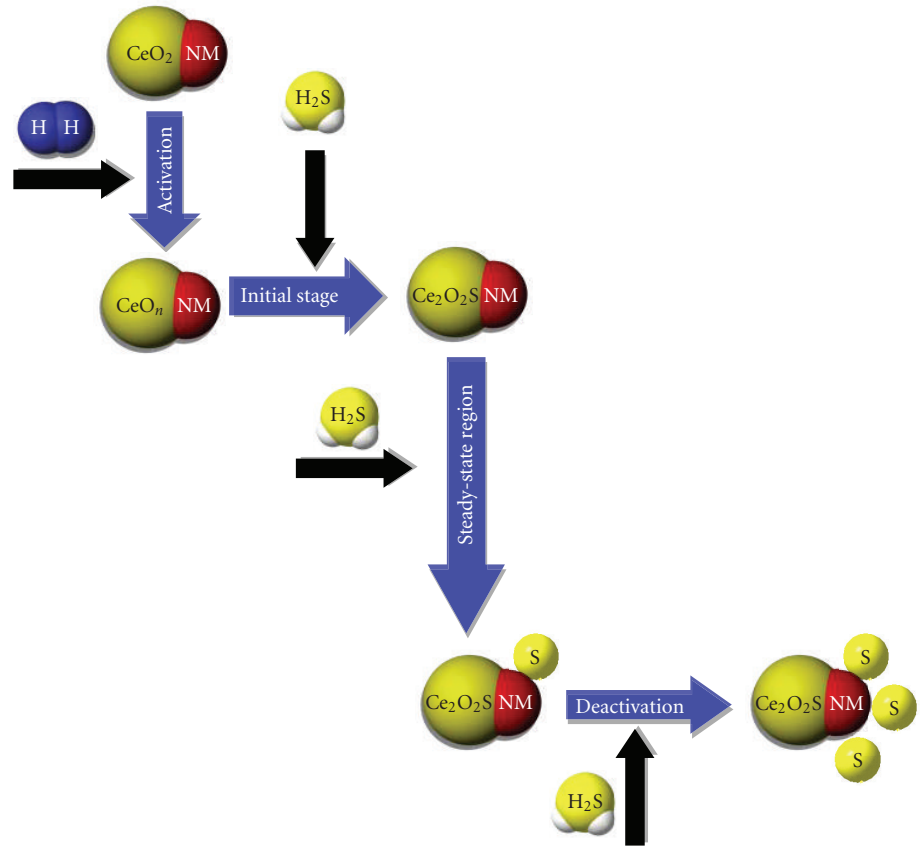

Figure 14: Phenomenological mechanism operative in the monometal supported catalysts.

shown below in the case of reaction (7a) for the purpose of illustration

$$4H_2 + CO_2 \longrightarrow CH_4 + 2H_2O, \tag{8}$$

$$K_{\text{eq}} = \exp\left(\frac{-\Delta G^{o}_{1073\text{K}}}{RT}\right) = \frac{y^{2}_{H_2O} \cdot y_{CH_4}}{y^{4}_{H_2} \cdot y_{CO_2}} = \frac{\varepsilon_e^{3} \cdot (5 - 2\varepsilon_e)^{2}}{64 \cdot (1 - \varepsilon_e)^{5}}, \tag{9}$$

where ε_e = the reaction fraction of each species at the steady-state.

At 800°C, ε_e is computed to be 0.862; the value of ε_e for reaction (7b) and (7c) is also calculated and is found to be 0.797 and 0.769, respectively, at the same temperature.

The equilibrium concentration of various species calculated for reactions represented in (7a)–(7c) is compared with the experimentally obtained data (Figure 15) in Table 2.

Understandably, the scheme proposed in (7c) is likely to be realistically closer to the conditions prevailing in the reformate than by (7a) or (7b). Consequently, as seen from Table 2, there is an excellent agreement (within±1%) between the theoretically predicted concentration of various components in the mixture and that determined experimentally, for reaction (7c). These results clearly explain and corroborate the rather high methane concentration and lower levels of CO and CO_2 found in the kerosene reformates.

In the light of the foregoing discussion, several multifunctional aspects of the catalysts developed in this work become evident. The nanostructured monometal-supported ceria formulations are capable of steam-reforming sulfur-laden (260 ppm) kerosene, resulting in very high hydrogen yield. Some key features of the sulfidation and reforming experiments of the monometal-supported formulations are as follows:

(a) Ruthenium-based formulation provided an excellent balance in hydrogen production and sulfur stability.

(b) Palladium-based formulation sorbed highest amounts of sulfur and also exhibited rapid and steady deactivation, thus suggesting that palladium has the highest propensity to sulfur poisoning.

(c) The rhodium-based formulation is most effective in hydrogen generation in terms of hydrogen yield and long-term stability.

(d) Ceria support plays a crucial role in rendering the catalyst sulfur tolerant and allowing the generation of hydrogen in high yield.

The on-stream long-term stability of these catalysts is due to their superior sulfur-tolerance without the need of *a priori* desulfurization stage; in the case of a real fuel such as kerosene which is a surrogate of JP-8, this aspect has hitherto not been examined or reported in the literature. Fukunaga

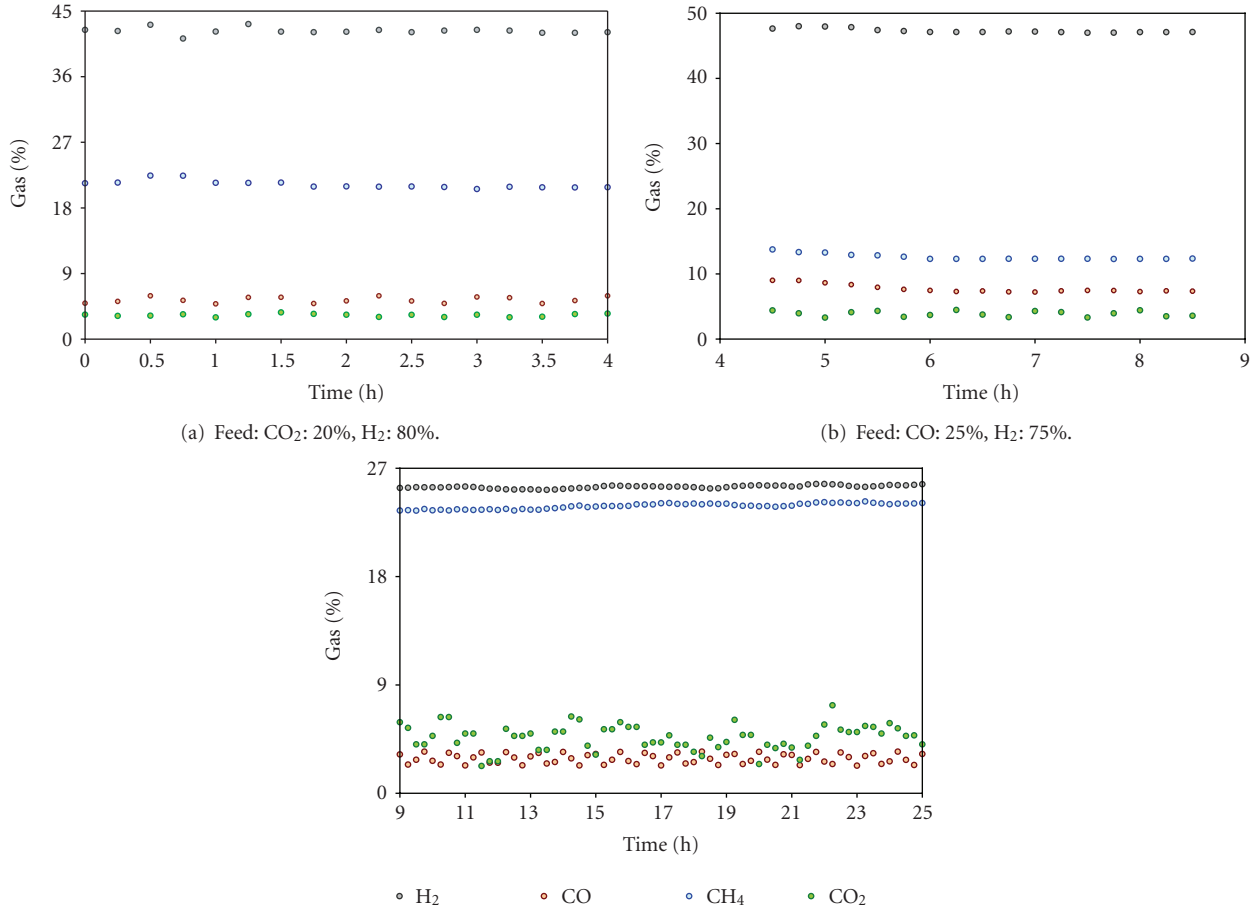

Figure 15: Evidence of the proposed in-situ methanation of carbon monoxide and carbon dioxide by hydrogen as per reactions (7a)–(7c) on the Pd-supported catalyst developed in this work.

Table 2: Steady-state concentration (%) of the reactants and products of methanation process.

Reaction	H_2 concentration		CO_2 concentration		CO concentration		CH_4 concentration	
	Theo.	Exp.	Theo.	Exp.	Theo.	Exp.	Theo.	Exp.
(7a)	16.9	42.3	4.2	3.3	—	5.4	26.3	21.2
(7b)	25.3	47.3	—	3.9	8.4	7.7	33.1	12.6
(7c)	27.3	25.5	3.9	4.7	3.9	2.9	26.0	23.9

et al. [42] have discussed the performance of a combined Ni-based desulfurizer and a Ru-supported alumina catalyst in the steam reforming of kerosene containing 48–64 ppm sulfur at 730°C. Even with the sulfur level reduced to about 0.05 ppm by desulfurization, the hydrogen level was ~70% with CO between 12–15% and CO_2 between 15–18% in the reformate. It can be reasonably argued that with pre-reforming desulfurization, the catalysts developed in this work would perform even better.

The catalysts are also capable of in-situ methanation of carbon monoxide and carbon dioxide in the presence of hydrogen—a feature also not reported in the literature with regard to fuel reforming. This aspect is unique and relevant in the context of eliminating CO and CO_2, thereby obviating the need of separate and elaborate stages for CO removal and CO_2 sequestration and/or capture. Fukunaga et al. [42] had employed a water-gas-shift reaction to remove CO from the stream.

The observed behavior of in-situ methanation is common to all the three formulations irrespective of the type of precious metal supported on the GDC matrix. Thus, it can be concluded that this is an artifact of the novel combination of the precious metal(s) with doped ceria support, both being endowed with nanofeatures. A recent study on methanation of carbon oxides used a catalyst that contains 9–16% Ru on γ-Al_2O_3 [43]. Methanation of CO in hydrogen rich gas mixture was also reported using catalysts containing 10% of several metals (Pt, Pd, Co, Ni, and Ru) over SiO_2 support

[44]. Some studies using 7–10% NiO on TiO_2 and γ-Al_2O_3 for the methanation of carbon oxides in hydrogen-rich stream catalysts have also been reported [45–47].

As can be seen, these studies employ very high loading of Ni and other noble metals, all of which are quite expensive (in addition to Ni being prone to carburization), whereas the catalysts developed in this research contain 1% of the noble metal and are capable of performing in-situ methanation in addition to generating hydrogen in high yield.

4. Conclusion

A new family of high performance monometal-supported ceria nanocatalysts has been developed and systematically characterized with respect to their structural, microstructural and sulfur-tolerance aspects. Steam-reforming of kerosene at 800°C and atmospheric pressure with steam-to-carbon (S/C) ratio equal to 3.0 on these formulations produces hydrogen-rich reformates over long durations before deactivation sets in, which is rather slow and monotonic than sudden and precipitous. The difference in the behavior of various formulations is explained in terms of the inherent ability of the ceria support to pick-up sulfur in the stream. This together with the sulfidation propensity of the precious metals dispersed on ceria is the reason behind excellent performance of these formulations. The catalyst deactivation appears mainly due to the sulfur poisoning rather than carburization (coke formation) based on the absence of noticeable level of elemental carbon in high resolution microscopic images in the postreformed samples. A mechanistic scheme for the phenomenon of in-situ methanation is also proposed which successfully explains the experimental data.

References

[1] J. Verne, *The Mysterious Island*, 1874, http://www.literature-web.net/verne/mysteriousisland.

[2] C. Song, "Fuel processing for low-temperature and high-temperature fuel cells: challenges, and opportunities for sustainable development in the 21st century," *Catalysis Today*, vol. 77, no. 1-2, pp. 17–49, 2002.

[3] "Advanced technologies for the control of sulfur dioxide emissions from coal-fired boilers," Topical Report 12, NETL/DOE, June 1999.

[4] Y. Lu, J. Chen, Y. Liu, Q. Xue, and M. He, "Highly sulfur-tolerant $Pt/Ce_{0.8}Gd_{0.2}O_{1.9}$ catalyst for steam reforming of liquid hydrocarbons in fuel cell applications," *Journal of Catalysis*, vol. 254, no. 1, pp. 39–48, 2008.

[5] I. Alstrup, J. R. Rostrup-Nielsen, and S. Røen, "High temperature hydrogen sulfide chemisorption on nickel catalysts," *Applied Catalysis*, vol. 1, no. 5, pp. 303–314, 1981.

[6] J. R. Rostrup-Nielsen, "Production of synthesis gas," *Catalysis Today*, vol. 18, no. 4, pp. 305–324, 1993.

[7] T. Suzuki, H.-I. Iwanami, and T. Yoshinari, "Steam reforming of kerosene on Ru/Al_2O_3 catalyst to yield hydrogen," *International Journal of Hydrogen Energy*, vol. 25, no. 2, pp. 119–126, 2000.

[8] A. Trovarelli, Ed., *Catalysis by Ceria and Related Materials*, vol. 2, Imperial College Press, London, UK, 2002.

[9] *Handbook of Aviation Fuel Properties*, Coordinating Research Council, Atlanta, Ga, USA, 1983.

[10] M. Mogensen, N. M. Sammes, and G. A. Tompsett, "Physical, chemical and electrochemical properties of pure and doped ceria," *Solid State Ionics*, vol. 129, no. 1, pp. 63–94, 2000.

[11] M. Funabiki, T. Yamada, and K. Kayano, "Auto exhaust catalysts," *Catalysis Today*, vol. 10, no. 1, pp. 33–43, 1991.

[12] S. Tagliaferri, R. A. Köppel, and A. Baiker, "Influence of rhodium- and ceria-promotion of automotive palladium catalyst on its catalytic behaviour under steady-state and dynamic operation," *Applied Catalysis B*, vol. 15, no. 3-4, pp. 159–177, 1998.

[13] A.-M. Azad and M. J. Duran, "Development of ceria-supported sulfur tolerant nanocatalysts: Rh-based formulations," *Applied Catalysis A*, vol. 330, no. 1-2, pp. 77–88, 2007.

[14] A.-M. Azad, M. J. Duran, A. K. McCoy, and M. A. Abraham, "Development of ceria-supported sulfur tolerant nanocatalysts: Pd-based formulations," *Applied Catalysis A*, vol. 332, no. 2, pp. 225–236, 2007.

[15] A. C. McCoy, M. J. Duran, A.-M. Azad, S. Chattopadhyay, and M. A. Abraham, "Performance of sulfur tolerant reforming catalysts for production of hydrogen from jet fuel simulants," *Energy and Fuels*, vol. 21, no. 6, pp. 3513–3519, 2007.

[16] ICDD card # 75-0162.

[17] A. Kataria, P. Ayyappan, and M. Abraham, "Effective sulfur tolerant catalyst for steam reforming of jet fuel," in *Proceedings of the AIChE Annual Meeting*, Salt Lake City, Utah, USA, November 2007.

[18] D. H. Kim, J. S. Kang, Y. J. Lee et al., "Steam reforming of n-hexadecane over noble metal-modified Ni-based catalysts," *Catalysis Today*, vol. 136, no. 3-4, pp. 228–234, 2008.

[19] D. J. Moon, J. W. Ryu, S. D. Lee, B. G. Lee, and B. S. Ahn, "Ni-based catalyst for partial oxidation reforming of *iso*-octane," *Applied Catalysis A*, vol. 272, no. 1-2, pp. 53–60, 2004.

[20] J. Thormann, L. Maier, P. Pfeifer, U. Kunz, O. Deutschmann, and K. Schubert, "Steam reforming of hexadecane over a Rh/CeO_2 catalyst in microchannels: experimental and numerical investigation," *International Journal of Hydrogen Energy*, vol. 34, no. 12, pp. 5108–5120, 2009.

[21] M. Wojciechowska, M. Pietrowski, and S. Łomnicki, "Novel supported catalyst for hydrodesulfurization reaction," *Chemical Communications*, vol. 35, no. 5, pp. 463–464, 1999.

[22] T. A. Pecoraro and R. R. Chianelli, "Hydrodesulfurization catalysis by transition metal sulfides," *Journal of Catalysis*, vol. 67, no. 2, pp. 430–445, 1981.

[23] M. Wojciechowska, M. Pietrowski, B. Czajka, and S. Łomnicki, "Influence of activation and the HDS reaction on the structure of magnesium fluoride-supported Ru catalysts derived from ruthenium chloride hydrate," *Catalysis Letters*, vol. 87, no. 3-4, pp. 153–157, 2003.

[24] http://www.chemistry.bnl.gov/nanocatalysis/research/imaging/imaging.htm.

[25] A. Ishiguro, T. Nakajima, T. Iwata et al., "Nanoparticles of amorphous ruthenium sulfide easily obtainable from a TiO_2-supported hexanuclear cluster complex $[Ru_6C(CO)_{16}]^{-2}$: a highly active catalyst for the reduction of SO_2 with H_2," *Chemistry—A European Journal*, vol. 8, no. 14, pp. 3260–3268, 2002.

[26] R. R. Chianelli, "Periodic trends transition metal sulfide catalysis: intuition and theory," *Oil and Gas Science and Technology*, vol. 61, no. 4, pp. 503–513, 2006.

[27] V. Meng and D. A. R. Kay, in *Proceedings of the World Congress on High Tech Ceramics, the 6th International Meeting on Modern Ceramic Technologies*, P. Vincenzini, Ed., Elsevier, Milan, Italy, 1986.

[28] R. M. Ferrizz, R. J. Gorte, and J. M. Vohs, "Determining the Ce_2O_2S-CeO_x phase boundary for conditions relevant to adsorption and catalysis," *Applied Catalysis B*, vol. 43, no. 3, pp. 273–280, 2003.

[29] K. Yi, *Ceria-zirconia oxide high temperature desulfurization sorbent*, Ph.D. dissertation, Louisiana State University, Baton Rouge, La, USA, 2004.

[30] R. S. Kempegowda, N. Laosiripojana, and S. Assabumrungrat, "High temperature desulfurization over nano-scale high surface area ceria for application in SOFC," *Korean Journal of Chemical Engineering*, vol. 25, no. 2, pp. 223–230, 2008.

[31] T. Ino, I. Anzai, and Y. Fujino, "Catalysts for the high-temperature steam reforming of hydrocarbons," US patent no. 5268346, 1993.

[32] M. Asadullah, S.-I. Ito, K. Kunimori, M. Yamada, and K. Tomishige, "Biomass gasification to hydrogen and syngas at low temperature: novel catalytic system using fluidized-bed reactor," *Journal of Catalysis*, vol. 208, no. 2, pp. 255–259, 2002.

[33] J. Zheng, J. J. Strohm, and C. Song, "Steam reforming of liquid hydrocarbon fuels for micro-fuel cells. Pre-reforming of model jet fuels over supported metal catalysts," *Fuel Processing Technology*, vol. 89, no. 4, pp. 440–448, 2008.

[34] Z. Wu, D. Huang, X. Yang et al., "Identification of induced reaction during XPS depth profile measurements of CeO_2/Si films grown by ion beam epitaxy," *Vacuum*, vol. 49, no. 2, pp. 133–137, 1998.

[35] H. Ono, A. Iwase, N. Ishikawa, Y. Baba, and N. Hirao, "Study of high energy ion-radiation effects in CeO_2 by X-ray photoelectron spectroscopy," Photon Factory Activity Report 27A/2007G058, #27, 2008.

[36] E. Bêche, P. Charvin, D. Perarnau, S. Abanades, and G. Flamant, "Ce 3d XPS investigation of cerium oxides and mixed cerium oxide ($Ce_xTi_yO_z$)," *Surface and Interface Analysis*, vol. 40, no. 3-4, pp. 264–267, 2008.

[37] J. F. Moulder, W. F. Stickle, P. E. Sobol, K. D. Bomben, J. Chastain, and R. C. King, *Handbook of X-Ray Photoelectron Spectroscopy*, Physical Electronics, Eden Prairie, Minn, USA, 1995.

[38] C. Mun, J. J. Ehrhardt, J. Lambert, and C. Madic, "XPS investigations of ruthenium deposited onto representative inner surfaces of nuclear reactor containment buildings," *Applied Surface Science*, vol. 253, no. 18, pp. 7613–7621, 2007.

[39] A. Gayen, K. R. Priolkar, P. R. Sarode et al., "$Ce_{1-x}Rh_xO_{2-\delta}$ solid solution formation in combustion-synthesized Rh/CeO_2 catalyst studied by XRD, TEM, XPS, and EXAFS," *Chemistry of Materials*, vol. 16, no. 11, pp. 2317–2328, 2004.

[40] D. Shekhawat, D. Berry, T. H. Gardner, and J. J. Spivey, "Catalytic reforming of liquid hydrocarbon fuels for fuel cell applications," *Catalysis*, vol. 19, pp. 184–254, 2006.

[41] J. M. Smith, H. V. Van Ness, and M. M. Abbott, *Introduction to Chemical Engineering Thermodynamics*, chapter 13, McGraw–Hill, New York, NY, USA, 7th edition, 2005.

[42] T. Fukunaga, H. Katsuno, H. Matsumoto, O. Takahashi, and Y. Akai, "Development of kerosene fuel processing system for PEFC," *Catalysis Today*, vol. 84, no. 3-4, pp. 197–200, 2003.

[43] Z. Kowalczyk, K. Stołecki, W. Raróg-Pilecka, E. Miśkiewicz, E. Wilczkowska, and Z. Karpiński, "Supported ruthenium catalysts for selective methanation of carbon oxides at very low Co_x/H_2 ratios," *Applied Catalysis A*, vol. 342, no. 1-2, pp. 35–39, 2008.

[44] V. Stuchly and K. Klusacek, "Unsteady-state carbon monoxide methanation on an Ni/SiO_2 catalyst," *Journal of Catalysis*, vol. 139, no. 1, pp. 62–71, 1993.

[45] L. C. Loc, N. M. Tuan, N. K. Dung, N. N. H. Phuc, and H. S. Thoang, "A study on methanation of carbon monoxide over catalysts NiO/TiO_2 and NiO/γ-Al_2O_3," *Advanced, Nature, Science*, vol. 7, pp. 91–105, 2006.

[46] M. Marwood, R. Doepper, and A. Renken, "In-situ surface and gas phase analysis for kinetic studies under transient conditions: the catalytic hydrogenation of CO_2," *Applied Catalysis A*, vol. 151, no. 1, pp. 223–246, 1997.

[47] N. W. Cant and A. T. Bell, "Studies of carbon monoxide hydrogenation over ruthenium using transient response techniques," *Journal of Catalysis*, vol. 73, no. 2, pp. 257–271, 1982.